split as

$$\Sigma'^{1}_{ijk} = \Sigma^{1i}_{ijk} + \Sigma^{1s}_{ijk} \quad (45)$$

into an i tensor Σ^{1i} and an s tensor Σ^{1s}, both of which are third-rank tensors without intrinsic symmetry. Σ'''^{1} can be expressed in terms of these tensors as

$$\Sigma'''^{1}_{jik} = -\Sigma^{1i}_{ijk} + \Sigma^{1s}_{ijk}. \quad (46)$$

3. Discussion

In contrast to tensors describing equilibrium properties, tensors describing transport properties generally split into two components behaving differently under 1′ if the point group is not grey. If one of the two components is symmetric under the exchange of the two indices that do not refer to **H**, the other will be antisymmetric in these indices.

Some authors (Cracknell, 1973; Birss & Fletcher, 1980; Malinowski, 1986) let **H** include internal magnetic fields generated by the magnetic structure in addition to the externally applied magnetic field. Although both types of magnetic field behave in the same way under time reversal, there are essential differences, which require separate treatment in order to avoid confusion. Externally applied magnetic fields may be chosen to be arbitrarily small so that an extension into powers of **H** does make sense, which is not the case for internal fields, *e.g.* in a magnetic domain of a single crystal of ferromagnetic material. The internal field of such a domain is invariant under the symmetry group of the domain whereas **H** may have any direction.

Our treatment of transport properties is compatible with the treatment of magneto-optic effects in magnetically ordered crystals by Eremenko & Kharchenko (1984). The optical properties also differ essentially from equilibrium properties because of the high frequencies that are involved.

The author is very grateful to Professors H. Schmid and J. Brandmüller for drawing his attention to transport properties in magnetically ordered crystals, for guiding him to relevant literature and for their constructive criticism of an earlier version of this paper.

References

Birss, R. R. (1964). *Symmetry and Magnetism.* Amsterdam: North-Holland.

Birss, R. R. & Fletcher, D. (1980). *J. Magn. Magn. Mater.* **15–18**, 915–916.

Butzal, H.-D. & Birss, R. R. (1982). *Physica (Utrecht)*, **A114**, 518–521.

Campbell, I. A. (1979). *J. Magn. Magn. Mater.* **12**, 31–33.

Cheremushkina, A. V. & Vasil'eva, R. P. (1966). *Fiz. Tverd. Tela (Leningrad)*, **8**, 822–825; Engl. transl: (1966). *Sov. Phys. Solid State*, **8**, 659–661.

Cracknell, W. H. (1973). *Phys. Rev. B*, **7**, 2145–2154.

Eremenko, V. V. & Kharchenko, N. F. (1984). *Sov. Sci. Rev. A*, **5**, 1–97.

Freimuth, A., Hohn, C. & Galffy, M. (1991). *Phys. Rev. B*, **44**, 10396–10399.

Grimmer, H. (1991). *Acta Cryst.* **A47**, 226–232.

Huebener, R. P. (1990). *Physica (Utrecht)*, **C168**, 605–608.

Kleiner, W. H. (1966). *Phys. Rev.* **142**, 318–326.

Kleiner, W. H. (1967). *Phys. Rev.* **153**, 726–727.

Kleiner, W. H. (1969). *Phys. Rev.* **182**, 705–709.

Kober, F., Ri, H.-C., Gross, R., Koelle, D., Huebener, R. P. & Gupta, A. (1991). *Phys. Rev. B*, **44**, 11951–11959.

Malinowski, S. (1986). *Acta Phys. Pol. A*, **69**, 33–43.

Nye, J. F. (1985). *Physical Properties of Crystals*, 2nd ed. Oxford: Clarendon.

Pourghazi, A. & Saunders, G. A. (1977). *Phys. Lett. A*, **62**, 521–522.

Pourghazi, A., Saunders, G. A. & Akgöz, Y. C. (1976). *Philos. Mag.* **33**, 781–784.

Shtrikman, S. & Thomas, H. (1965). *Solid State Commun.* **3**, 147–150; erratum (1965), **3**, civ.

Thomas, H. (1965). *Z. Angew. Phys.* **18**, 404–414.

Varlamov, A. A. & Livanov, D. V. (1991). *Zh. Eksp. Teor. Fiz.* **99**, 1816–1826; Engl. transl: (1991). *Sov. Phys. JETP*, **72**, 10 16–1022.

Zavaritsky, N. V., Samoilov, A. V. & Yurgens, A. A. (1991). *Physica (Utrecht)*, **C180**, 417–425.

Acta Cryst. (1993). A**49**, 771–781

X-ray Scattering from Systems in Early Stages of Precipitation

By C. R. Houska

Department of Materials Engineering, Virginia Polytechnic Institute and State University, Blacksburg, Virginia 24061, *USA*

(*Received* 12 *January* 1993; *accepted* 15 *April* 1993)

Abstract

Certain age-hardenable alloy systems can produce zones of large matrix distortion about precipitates having a size misfit with the surrounding matrix. These zones grow with ageing and give diffraction effects that are challenging to interpret. This paper describes such a model, based upon the random

positioning of precipitates that produce severely distorted zones in the surrounding matrix. In an intermediate stage, matrix intensity is partitioned into Bragg peaks, static diffuse scattering and quasilines. The latter two forms of scattering are diffuse scattering that sharpens to widths not much broader than those of normal Bragg peaks. When all three forms of scattering are present, they are sufficiently localized about the reciprocal-lattice points to allow a column interpretation of the diffraction model much like that used in the study of cold-worked metals. The strain Fourier coefficients in this case are calculated from an elastic model. Theoretical results include Laue-like scattering from precipitates, which can also be influenced by displacement fields from other precipitates. In this case, the dominance of particle-size broadening reduces the role of strain broadening. Results may be expressed in terms of a few parameters that may be conveniently related to physical properties.

I. Introduction

When atoms in binary solid solutions are correlated over relatively small distances, diffuse scattering provides a proven method of determining the local atomic arrangements in terms of a limited number of short-range-order (SRO) and size-effect coefficients [see Moss, Sparks & Ice (1992*a*,*b*), Schwartz & Cohen (1987) and Warren (1969)]. However, for systems undergoing phase separation, the correlation distances and therefore the number of SRO coefficients soon become excessive as the transformation proceeds. Large displacements extending well outside a precipitate greatly complicate this approach and the determination of atomic arrangements becomes unnecessarily difficult. Under these conditions, the diffuse scattering sharpens into broadened Bragg-like peaks. The intent of this paper is to treat this early stage of precipitation in such a way that the structural parameters are limited in number and may be related more directly to the physical phenomena. This paper provides a theoretical basis for future papers dealing with experimental X-ray diffraction results obtained from various ageing treatments, to be reported, on a copper–beryllium sample. In this case, precipitation has produced severe distortions in the matrix about precipitates.

Age-hardening transformations in crystalline solids begin with finite transformed regions (clusters, zones or precipitates) that are between one and several orders of magnitude smaller than the dimensions of the original crystal. For systems having two or more atomic species, the precipitate can become enriched in at least one component, producing a depletion in the surrounding matrix. The matrix lattice appears to be continuous about the precipitates, essentially extending to its original dimensions. The atomic positions within coherent precipitates may be treated as matrix positions that have undergone a simple transformation of their original positions with no loss or gain of sites but with a change in composition. Atomic planes enter and leave precipitates continuously. These zones of precipitation are highly oriented relative to the surrounding matrix. At the other extreme, the zone of precipitation may lose or gain lattice sites and have partial or no continuity with respect to the lattice planes in the matrix. In each case, the surrounding matrix can become distorted, depending upon the new atomic arrangements, the atomic size differences and relaxations associated with the interface structure. An alloy may experience both extremes during a transformation as it forms various intermediate metastable precipitates.

Krivoglaz and co-workers [see Krivoglaz & Hao (1969) and Barabash & Krivoglaz (1978)] have carried out theoretical investigations of X-ray scattering from spherical coherent precipitates with lattice distortions. More recently, Barabash & Krivoglaz (1981) have extended these results to include an anisotropic elastic matrix. Dederichs (1971) confirmed and extended the early work of Krivoglaz and co-workers for large distortions. Others (Dobromyslov, 1976, 1980; Ganzhuila, Kozlova & Kokorin, 1981; Larson & Schmatz, 1974; Larson *et al.*, 1987) have carried out theoretical and experimental studies of the scattering from dilute and concentrated alloys containing precipitates. Trinkhaus (1971) treated the scattering from an isotropic distortion center in an isotropic material in the limit of vanishing defect sizes but with large distortions. The form for the scattering near the Bragg reflections was identified. Dederichs (1970) and Holý (1984) have discussed diffuse scattering for the case of inclusions with amorphous internal structure. These treatments generally make simplifying assumptions or approximations to achieve closed-form expressions for the scattering. Iida, Larson & Tischler (1988) have used numerical calculations to investigate the scattering near Bragg reflections from spherical coherent precipitates in an elastically isotropic medium, reducing the calculation to an easily evaluated one-dimensional numerical integral, which illustrates the characteristic form of the scattering from finite-sized precipitates. These results provide a determination of the size, internal strain and number density of such precipitates in crystalline materials that obey these conditions. However, the problem of large distortions leading to quasilines was not treated.

Explicit and detailed calculations are still needed for the analysis of experimental measurements from samples having precipitates of a more general shape, of finite size and producing severe displacements in an elastically anisotropic matrix. In the following

scattering calculations, a void is created by the subtraction of matrix atoms and refilled with atoms of the correct type and arrangement. A range of precipitate shapes may be treated by making use of an ellipsoid of revolution with various semi-axis ratios. Precipitates shaped as needles, spheres or discs are special forms of an ellipsoid. The displacement field in the matrix resulting from misfit is also conveniently determined with an ellipsoidal shape.

A quantitive X-ray diffraction analysis from samples containing a mixture of two crystalline phases can be approached using well established techniques [see Cullity (1978)]. However, when precipitation occurs within grains, as previously described, several additional scattering effects are found that are not of a routine nature. These effects are conveniently developed in three stages. The first is a calculation of the scattering from a matrix with voids in an otherwise continuous lattice. The second introduces precipitates into void space and the third treats the elastic disturbance about precipitates. A paper is in preparation that illustrates a quantitative application of diffraction theory developed in this paper to fit experimental data obtained from a copper–beryllium alloy.

II. Diffraction from voids

In calculating the scattering from a random distribution of n_v voids, it is assumed that the fraction of vacant sites is small, *i.e.* less than 1/20. The full amplitude of scattering may be described by a sum over all lattice sites.

$$A = F\sigma \tag{1a}$$

$$\sigma = \sum_m \exp(2\pi i\mathbf{H}\cdot\boldsymbol{\delta}_m)\exp(2\pi i\mathbf{H}\cdot\mathbf{R}_m), \tag{1b}$$

where F is the structure factor of a cell at lattice position R_m, given in terms of the average lattice parameters a_1, a_2 and a_3 and the cell displacements $\boldsymbol{\delta}_m$. The position in reciprocal space is given by

$$\mathbf{H} = h_1\mathbf{b}_1 + h_2\mathbf{b}_2 + h_3\mathbf{b}_3, \tag{2}$$

where h_1, h_2 and h_3 are continuous variables and $\mathbf{b}_1$, $\mathbf{b}_2$ and $\mathbf{b}_3$ are the reciprocal-lattice vectors determined by their average lattice. The presence of voids reduces the amplitude according to

$$A_v = F\left[\sigma - \sigma_v\sum_m^{n_v}\exp(2\pi i\mathbf{H}\cdot\boldsymbol{\delta}_m)\exp(2\pi i\mathbf{H}\cdot\mathbf{R}_m)\right], \tag{3a}$$

where the summation contains terms that locate the center of each void within the matrix lattice. σ_v represents a limited summation over fictitious matrix cells and is like (1*b*) but only taken over the fictitious set of matrix cells that must be removed in order to create a void. These fictitious cells are arranged like matrix cells with locations given in terms of the average matrix lattice parameters rather than the new set that is described later for precipitates.

The sum

$$\sigma_{cv} = \sum_m^{n_v}\exp(2\pi i\mathbf{H}\cdot\boldsymbol{\delta}_m)\exp(2\pi i\mathbf{H}\cdot\mathbf{R}_m)$$

extends over all center points of voids within the matrix lattice. This allows the amplitude of matrix scattering with voids to be written as

$$A_v = F[\sigma - \sigma_v\sigma_{cv}]. \tag{3b}$$

To calculate the intensity, I, in electron units, we average the product of amplitudes

$$I/F^2 = \langle AA^*\rangle = \langle(\sigma - \sigma_{cv}\sigma_v)(\sigma - \sigma_{cv}\sigma_v)\rangle. \tag{4}$$

The average for all grains is taken by allowing the center of each of the n_v voids to occupy each lattice position without considering impingements or lost sites at or near the surface. This is valid for small concentrations of voids – a restriction that is reconsidered later. In carrying out the summations σ and σ_v, it is convenient to locate both origins at centers of symmetry, *i.e.* in the lattice and the void. This results in the following relations for complex conjugates: $\sigma = \sigma^*$, $\sigma_v = \sigma_v^*$, $\sigma_{cv} = \sigma_{cv}^*$, such that

$$I/F^2 = \sigma^2 - 2\langle\sigma_{cv}\rangle\sigma_v\sigma + \langle\sigma_{cv}^2\rangle\sigma_v^2; \tag{5}$$

each void is taken to be identical with an average size. Because each of the n_v void centers can occupy all lattice sites independently, one can write

$$\sigma_{cv} = n_v(\sigma/N). \tag{6}$$

The average of the third term in (5) involves a double sum containing n_v^2 terms, which can be reduced to

$$\langle\sigma_{cv}^2\rangle = n_v + n_v(n_v - 1)(\sigma/N)^2 \tag{7}$$

for a random arrangement of voids. Substitution of (6) and (7) into (5) gives

$$I/F^2 = \sigma^2 - 2(n_v/N)\sigma_v\sigma^2 + n_v\sigma_v^2 + (n_v/N)^2\sigma_v^2\sigma^2, \tag{8}$$

with the approximation $n_v - 1 \simeq n_v$.

Equation (8) can be simplified if a precipitate has dimensions much smaller than every dimension in the crystal. With σ_v having a width that is one to two orders of magnitude broader than σ, the products become

$$\sigma_v\sigma^2 \simeq \sigma_v(M)\sigma^2, \tag{9}$$

$$\sigma_v^2\sigma^2 \simeq \sigma_v^2(M)\sigma^2, \tag{10}$$

where $\sigma_v(M)$ is taken as a constant and designates the value of σ_v at the peak position of the much sharper matrix function, σ.

With substitution of (9) and (10) into (8), or

$$I = F_{MV}^2\sigma^2 + NC_vF^2(\sigma_v^2/N_v), \tag{11a}$$

with

$$F_{MV}^2 = F^2\{1 - C_v[\sigma_v(M)/N_v]\}^2 \tag{11b}$$

and

$$C_v = n_v N_v / N,$$

F_{MV} can be taken as an average structure factor for a matrix with voids, while C_v is the fraction of fictitious matrix cells associated with voids.

The first term of (11*a*) represents the Bragg scattering with a modified structure factor that allows for the removal of cells at voids. If the displacements $\delta_m = 0$, the scattering is localized into sharp Bragg peaks scaled by F_{MV}^2 and shaped according to σ^2. Equation (11*a*) is rewritten and modified to

$$I/F^2 = N[(1-C_v)^2(\sigma^2/N) + NC_v(1-C_v)(\sigma_v^2/N_v)], \tag{12}$$

where

$$\sigma_v(M) = N_v.$$

This result could have been obtained directly by taking an average $\langle F \rangle$ over unit cells in the matrix and nonscattering void cells. The second term, or the void scattering, did not initially allow for void overlap in taking the sum over void positions and gives an overestimate of the void scattering. At this point, overlap is introduced as a linear correction. This accounts for the additional term, $(1-C_v)$, in (12), which takes the void scattering to zero as $C_v \rightarrow 1$ and does not alter the original result as $C_v \rightarrow 0$.

Another known limit can be examined by beginning with (12). If this is a random solution of matrix atoms with scattering factor f and vacancies, with $N_v = 1$, $F = f$ (1 atom cell^{-1}) making $\sigma_v^2 = 1$, one obtains the classical Laue monotonic scattering. Under these conditions, the second term is identically equal to the expected Laue monotonic (Warren, 1969) or

$$NC_v(1-C_v)(f-0)^2. \tag{13}$$

Omitting the overlap correction $(1-C_v)$, as in the initial development, would restrict the result to small values of C_v.

An integration of (12) over σ^2 and σ_v^2 gives

$$N(1-C_v),$$

the total number of occupied lattice cells. If the overlap correction were not included, a second-order term, NC_v^2, would remain uncancelled.

III. Scattering from precipitates

The results of the preceding section represent a starting point for calculation of the scattering from a lattice containing precipitates. In this case, the voids are filled with precipitates having a structure that in some way differs from the matrix. Lattice sites may or may not be conserved and an elastic disturbance in the matrix is included in σ as displacements, δ_m, that are obtained from an elastic model. As before, σ_v is a summation over fictitious matrix cells that are subtracted to make space for an average precipitate. σ_β is a summation over average precipitate cells occupying an average void having a structure factor F_β. The precipitate lattice parameters are a_1^β, a_2^β and a_3^β, with reciprocal axes $\mathbf{b}_1^\beta$, $\mathbf{b}_2^\beta$ and $\mathbf{b}_3^\beta$. Addition of the amplitudes to (3) gives the amplitude for a matrix with precipitates, *i.e.*

$$I = [F(\sigma - \sigma_{cv}\sigma_v) + F_\beta \sigma_{c\beta}\sigma_\beta] \times [F^*(\sigma - \sigma_{cv}\sigma_v) + F_\beta^* \sigma_{c\beta}\sigma_\beta^*]. \tag{14}$$

The same center locations are taken for voids and precipitates, such that $\sigma_{cv} = \sigma_{c\beta}$ and $\sigma_\beta = \sigma_\beta^*$ because the origins are at centers of symmetry. By using these relations and taking the product, one obtains

$$I = F_{MP}^2 \sigma^2 + n_\beta (F_\beta \sigma_\beta - F\sigma_v)^2, \tag{15a}$$

with

$$F_{MP} = F(1 + (C_v/N_v)\{[F_\beta(M)/F] \times \sigma_\beta(M) - \sigma_v(M)\}), \tag{15b}$$

where n_β is the number of precipitates, which is equal to the number of voids, n_v. Note that the structure factor F_{MP} for the matrix is altered if the scattering amplitude of the precipitate has a nonzero value at the Bragg peak for the matrix. The degree of overlap determines the coherency at the sharp Bragg peak originating from the matrix due to precipitate scattering. It also includes a negative contribution from the fictitious matrix cells in that volume occupied by precipitates. The second term in (15*a*), when expanded as a binomial, contains relatively broad Bragg scattering from the precipitate, void scattering and a cross term. It reduces to the classical Laue monotonic diffuse scattering if the precipitates each contain only one atom, *B*, in a matrix of *A* atoms.

Equation (15*a*) can be rewritten as the intensity per cell:

$$I/N = F_{MP}^2(\sigma^2/N) + C_v(1-C_v)(1/N_v) \times (F_\beta \sigma_\beta - F\sigma_v)^2, \quad C_v < 0.5. \tag{16}$$

Again, a linear impingement correction $(1-C_v)$ is included. The two reciprocal lattices, one for the matrix and one for the precipitate, are typically related by orientation relationships in the early stages of precipitation. Orientation relationships, differences in the reciprocal-lattice vectors and the ratio $C_v F_\beta(M)\sigma_\beta(M)/N_v F\sigma_v(M)$ determine the coherency correction contained in F_{MP}.

Equation (16) agrees with four limits that are listed as follows:

(I) The first limit is taken by setting $F_\beta = 0$, which gives the void limit considered in the preceding section, *i.e.* (12).

(II) Matrix without precipitates. In the second limit, voids and precipitates are eliminated by

refilling voids with matrix material. This requires $F_\beta = F$ and $\sigma_\beta = \sigma_v$, giving $I = F^2\sigma^2$.

(III) For the third limit of practical interest, the precipitate size and the lattice are sufficiently large and different for there to be no significant overlap between σ_v, σ_β and σ, causing $\sigma_\beta(M) = \sigma_\beta\sigma_v = 0$, which gives

$$I/N = F^2\{1 - C_v[\sigma_v(M)/N_v]\}^2(\sigma^2/N) + C_v(1 - C_v)\{[(F_\beta\sigma_\beta)^2/N_v] + [(F\sigma_v)^2/N_v]\}, \quad C_v < 0.5. \tag{17}$$

This represents a departure from the result typically used in conventional quantitative phase analysis owing to a void correction.

(IV) Laue monotonic. The fourth limit demonstrates that (16) is in agreement with the classical Laue monotonic scattering for a random solid solution of B atoms in a matrix of A atoms. This is found by setting $C_v = C_\beta$, $N_v = 1$, $\sigma_\beta = 1$, $F_\beta = f_B$ and $F = f_A$, giving

$$I = F_M^2\sigma^2 + C_v(1 - C_v)N(f_B - f_A)^2.$$

Again, complete agreement in this limit is found only when the impingement correction, $1 - C_v$, is included.

IV. Scattering from highly distorted lattices with precipitates

Lattice distortion associated with precipitation in an elastically anisotropic medium can become severe and produce special scattering effects. Little is known about the stage of growth when precipitates produce severe matrix distortions that begin to encompass a significant volume fraction of the matrix. This region of severe distortion can give Bragg-like quasiline peaks that are sharp enough to be misinterpreted as scattering from a new phase. However, a careful examination of their integrated intensities demonstrates that these scattering peaks originate from the matrix rather than from a new phase. As the volume fraction of severely distorted matrix increases, this scattering (the quasilines) increases in intensity. The quasiline peak width in a powder pattern is comparable to those of Bragg peaks measured from a highly cold worked metal. This similarity justifies a development that begins with a conventional powder line-shape calculation. It introduces mathematical simplicities at an early stage of the calculation. Lattice displacements are described later in terms of the ellipsoidal elastic model, which requires numerical calculations. At an intermediate stage of displacement severity, computer simulations show that Huang scattering is typically two to three times sharper than the quasilines and is located very close to the sharp Bragg peaks. Quasilines may be located anywhere, from the Bragg peaks of the pure solvent lattice to those positions expected from a random solid solution. The shape of precipitate scattering is assumed to be dominated by their small size, but internal displacements within precipitates, originating from secondary precipitates, may produce further broadening. As expected, the overall intensity of quasilines also increases with volume fraction.

The total matrix scattering power for one peak from a flat diffractometer sample (Warren, 1969; Schwartz & Cohen, 1987) is given by an integration over a small region in reciprocal space at distances h_1', h_2' and h_3' about a point (hkl):

$$P_M = I_e\{(1/\Delta V)[(A_0/2\mu)(\Omega/4\pi)jg_i]\}(R^2\lambda^3/V_c) \times \iiint[I_M(h_1'h_2'h_3')/\sin 2\theta]\,dh_1'\,dh_2'\,dh_3', \tag{18}$$

where I_e is the classical scattering from an electron, ΔV is the volume of an average, Ω is the solid angle of scattering viewed by the diffractometer out of a total angle of 4π, R is the sample–receiver-slit distance, λ is the wavelength, θ is the Bragg angle and

$$I_M(h_1'h_2'h_3') = F_{MP}^2\sigma^2, \tag{19}$$

with σ in its general form given by (1*b*). All other terms are defined in § V. For the present, it is sufficient to indicate that the terms in the curly brackets of (18) may be taken as the effective number of diffracting grains in a flat polycrystalline diffractometer sample, *i.e.*

$$(A_0/2\mu)(\Omega/4\pi)jg_i/\Delta V = \text{diffracting volume/volume of average grain.} \tag{20}$$

As previously discussed, the Bragg-like scattering is sufficiently close to the reciprocal-lattice points for the intensity integration in (18) to be performed over planes perpendicular to the diffraction vector, **H**, *i.e.* along $\mathbf{b}_1\mathbf{b}_2$ directions rather than over a sphere. This introduces simplifications in the interpretation of all results that follow the integration. That is, one considers the scattering between pairs of cells within columns perpendicular to the Bragg planes. For cubic systems, the interplanar spacing is given by

$$d = a/(h^2 + k^2 + l^2)^{1/2} = a_3/l_0, \tag{21}$$

with the normal Miller indices (hkl) representing the lowest order ($l_0 = 1$) for sets of planes of like orientation. a_3 is determined from the lattice parameter, a, of the normal cubic cell and h, k and l. Higher orders are designated by (nh, nk, nl) with $l_0 = n$. The basic unit of distance along a column, $d = a_3$, determines $(m_3 - m_3')a_3$, the separation distance between pairs of cells at m_3, m_3'. All distances and displacements entering into the intensity calculations become projected along specified columns normal to the reflecting planes. The location of the undisplaced origin of

the unit cell at $m_1m_2m_3$ is given by

$$\mathbf{R}(m) = m_1\mathbf{a}_1 + m_2\mathbf{a}_2 + m_3\mathbf{a}_3, \tag{22}$$

with an unprojected displacement

$$\boldsymbol{\delta}(m) = X_m\mathbf{a}_1 + Y_m\mathbf{a}_2 + Z_m\mathbf{a}_3, \tag{23}$$

which is independent of the kind of atom at m. Because we are only interested in projected displacements along $\mathbf{a}_3$, which are parallel to the reciprocal axis $\mathbf{b}_3$, the square of the amplitude is reduced to (Warren, 1969)

$$\sigma^2 = \sum_{m_1}\sum_{m_2}\sum_{m_3}\sum_{m_3'}\exp[2\pi i(Z_{m_3} - Z_{m_3'})l_0] \times \exp[2\pi i(m_3 - m_3')h_3], \tag{24}$$

which may be written in terms of an average over a representative grain for like pairs separated by $m_3 - m_3' = n$ cells:

$$(\sigma^2/N) = \sum_{m_3}\sum_{m_3'}(N_n/N_3)\langle\exp[2\pi i(Z_{m_3} - Z_{m_3'})l_0]\rangle_n \times \exp[2\pi i(m_3 - m_3')h_3], \tag{25}$$

where N_n is the total number of nth neighbors per column of orientation $[hkl]$ per grain, N_3 is the number of cells per column and N is the number of cells per grain. Since we are dealing with point-like defects having displacement fields falling off rapidly with distance relative to the size of a grain, at sufficiently large column distances, na_3, Z_{m_3} and $Z_{m_3'}$ become uncorrelated and may be averaged independently, *i.e.*

$$\langle\exp[2\pi i(Z_{m_3} - Z_{m_3'})l_0]\rangle = \langle\exp(2\pi iZ_{m_3}l_0)\rangle\langle\exp(-2\pi iZ_{m_3'}l_0)\rangle$$

Splitting (25) into correlated and uncorrelated terms gives a separation of Bragg and diffuse scattering:

$$\begin{aligned}(\sigma^2/N) = {} & \sum_{m_3}\sum_{m_3'}(N_n/N_3)\langle\exp(2\pi iZ_{m_3}l_0)\rangle \\ & \times\langle\exp(-2\pi iZ_{m_3'}l_0)\rangle\exp(2\pi inh_3) \\ & + \sum_{m_3}\sum_{m_3'}(N_n/N_3)[\langle\exp[2\pi i(Z_{m_3} - Z_{m_3'})l_0]\rangle \\ & - \langle\exp(2\pi iZ_{m_3}l_0)\rangle \\ & \times\langle\exp(-2\pi iZ_{m_3'}l_0)\rangle]\exp(2\pi inh_3).\end{aligned} \tag{26}$$

The second sum converges more rapidly than the first, *i.e.* well before $(N_n/N_3)\to 0$.

Displacements result from randomly positioned precipitates at sites t having a limited number of orientations that determine the overall symmetry of the deformed crystal. Ellipsoids located at lattice sites at m_1'', m_2'', m_3'', about a pair m_3, m_3', give additive displacements according to

$$Z_{m_3} = \sum_t x_tZ_{tm_3}, \tag{27}$$

with $x_t = 1$ or 0 depending upon whether a site is occupied or unoccupied by a center. The correlated average is considered first and carried out in terms of the probability of site occupancy, c, or $1 - c$ for an unoccupied site. Because the displacements Z_{m_3} weighted by l_0 can be large, no restrictive assumptions can be made about the magnitude of $l_0Z_{m_3}$. We substitute (27) into (26).

$$\left\langle\exp\left[2\pi i\sum_t l_0x_t(Z_{tm_3} - Z_{tm_3'})\right]\right\rangle = \left\langle\prod_t\exp[2\pi il_0x_t(Z_{tm_3} - Z_{tm_3'})]\right\rangle$$

and note that, if no displacement source is found at site t, $Z_{tm_3} = Z_{tm_3'} = 0$. The average for each term in the product becomes

$$x = 1 + c\{\exp[2\pi il_0(Z_{tm_3} - Z_{tm_3'})] - 1\}.$$

Using the logarithmic identity $x = \exp(\ln x)$ for each term in the product, one obtains

$$\exp[\ln(1 + c\{\exp[2\pi il_0(Z_{tm_3} - Z_{tm_3'})] - 1\})]. \tag{28}$$

Without restricting the values of $l_0Z_{m_3}$, one finds that

$$c\{\exp[2\pi il_0(Z_{tm_3} - Z_{tm_3'})] - 1\} \ll 0 \tag{29}$$

because $c \ll 1$ and the magnitude of terms in the brackets can only range from zero to one. Only one term of a series expansion of the logarithmic exponent is needed to treat large displacements. This important treatment for large $l_0Z_{m_3}$ values was first given by Krivoglaz (1959, 1960, 1961) and later by Dederichs (1971). Substitution back into (28) and reintroduction of the sum over t gives

$$\exp\left(-c\sum_t\{1 - \exp[2\pi il_0(Z_{tm_3} - Z_{tm_3'})]\}\right) = \exp(-T_{m_3m_3'}), \tag{30}$$

which also defines the exponential factor $T_{m_3m_3'}$.

This requires a detailed knowledge of a full set of relative displacements – a sizeable file of numbers. Consequently, the calculations are modified into a form involving displacements produced by a single particle interacting with columns. As a first step toward attaining this goal, (30) is rewritten as an equivalent product and sum, *i.e.*

$$\begin{aligned}-T_{m_3m_3'} = c\sum_t\{ & [\exp(2\pi il_0Z_{tm_3}) - 1] \\ & \times[\exp(-2\pi il_0Z_{tm_3'}) - 1] \\ & + [\exp(2\pi il_0Z_{tm_3}) - 1] \\ & + [\exp(-2\pi il_0Z_{tm_3'}) - 1]\}.\end{aligned} \tag{31}$$

The last two terms are simplified to

$$2c\sum_t[1 - \cos(2\pi l_0Z_{tm_3})] = 2M. \tag{32}$$

Initially, combinations of cells m_3, m_3' are selected having a column separation of n and with precipitate centers positioned in all possible lattice positions

about a pair. Alternatively, a single precipitate may be fixed at the center of coordinates and all displacements of matrix cells separated by n are summed throughout a crystal. The following exponential function describes terms for all correlated nth neighbors as well as terms that can be treated independently

$$-T(n) = \varphi(n) - 2M, \tag{33a}$$

with

$$\varphi(n) = c\sum_{m_1}\sum_{m_2}\sum_{m_3}[\exp(2\pi i l_0 Z_{m_3}) - 1] \times [\exp(-2\pi i l_0 Z_{m_3+n}) - 1], \tag{33b}$$

$$2M = 2c\sum_{m_1}\sum_{m_2}\sum_{m_3}[1 - \cos(2\pi l_0 Z_{m_3})]. \tag{33c}$$

The location of m_3 relative to the center of the precipitate t is given in terms of its vector components by $m_1\mathbf{a}_1 + m_2\mathbf{a}_2 + m_3\mathbf{a}_3$, while m_3' is located by simply adding $n\mathbf{a}_3$. Both are in a column at $m_1\mathbf{a}_1 + m_2\mathbf{a}_2$. Each neighbor n for all reflecting columns in the powder influences the value of $T(n)$ through the summation over m_1, m_2 and m_3 in a 'representative' crystal.

In treating the terms

$$\langle\exp(2\pi i l Z_{m_3})\rangle\langle\exp(-2\pi i Z_{m_3'})\rangle$$

found in the Bragg-peak equation (26), the averaging sequence described in (27)–(32) is used, except that cell displacements are treated separately. This gives the important attenuation term, $\exp(-2M)$, with the exponential factor described by (32).

Combination of terms and substitution into (26) gives

$$\sigma^2/N = \exp(-2M)\left(\sum_n (N_n/N_3)\exp(2\pi i n h_3) + \sum_n (N_n/N_3)\{\exp[\varphi(n)] - 1\}\exp(2\pi i n h_3)\right). \tag{34}$$

The first of these terms represents the Bragg peak, which can be strongly attenuated through the $2M$ factor. The second term represents the local diffuse scattering resulting from both large and small displacements.

At this point, it is convenient to re-examine the behavior of $\varphi(n)$ within two regions about a precipitate. In the second, small correlated elastic disturbances extending to distances greater than the highly disturbed zone about precipitates give a sizeable volume of coupling obeying the condition $\varphi(n) \ll 1$. The first region, or severely distorted zone, is also coupled, but displacements of m_3m_3' pairs are treated rigorously in the calculation of $\varphi(n)$ [see (28)–(30)]. It is a zone that surrounds individual precipitates, where coupling is largely influenced by the field from a single precipitate rather than from several, giving an additive displacement. Although (34) treats both large and small displacements, the procedure followed makes it necessary to distinguish between the two kinds of displacement zone because each gives distinguishable scattering phenomena. In view of the conditions placed upon the second region, the expansion

$$\{\exp[\varphi(n)] - 1\} \simeq \varphi(n) \tag{35}$$

is used. Equation (35) requires that the sum of products, with displacements located in the exponential terms of (33b), give a small $\varphi(n)$. At this point, the terms $2\pi l_0 Z_{m_3}$ are not assumed to be small. This gives the following static diffuse (SD) scattering that includes what is normally considered Huang* and Stokes–Wilson scattering, *i.e.*

$$I_{SD}/N = F_{MP}^2\exp(-2M)\sum_n (N_n/N_3)\varphi(n)\exp(2\pi i n h_3'). \tag{36}$$

Apart from the size coefficient, which typically converges more slowly than $\varphi(n)$, the summation is equivalent to the Fourier transformation of $\varphi(n)$ defined by $\varphi(h_3)$.

The quasiline can be isolated from other forms of diffuse scattering by the addition and subtraction of $\varphi(n)$ coefficients in the overall diffuse scattering, as given by the second term of (34), *i.e.*

$$\sigma^2/N = \exp(-2M)\left\{\sum_n (N_n/N_3)\exp(2\pi i n h_3) + \sum_n (N_n/N_3)\{\exp[\varphi(n)] - 1 - \varphi(n)\} \times \exp(2\pi i n h_3) + \sum_n (N_n/N_3)\varphi(n)\exp(2\pi i n h_3)\right\}. \tag{37}$$

The second summation is influenced by the severely distorted zone and, because $\varphi(n)$ has a complex component, it is typically shifted from the Bragg peak. Although $\varphi(n)$ is influenced by large displacements, this term cancels for small n owing to the addition and subtraction of $\varphi(n)$ terms in (37).

In evaluating the Fourier coefficients of the third summation, one finds that they converge more slowly than those in the second summation but faster than those coefficients describing the Bragg peak. Displacements that are weak but of sufficient strength to correlate pairs of cells within the columns play a dominant role in the static diffuse scattering because of their large numbers. However, additive terms that were subtracted from the second term (quasiline) are included as Fourier coefficients in the static diffuse scattering, *i.e.* for $\varphi(n < n_s)$. These are also

* It is not necessary to complicate this theory further by isolating Huang scattering but it could be done by treating the product $2\pi l_0 Z_{m_3}$ as a small quantity. Expansion of this as a linear term and addition and subtraction of this term in (37) introduces the Huang scattering. Details of this additional expansion may be found in Dederichs (1971).

determined by the severely distorted zone but play a less important role in the SD scattering because of their smaller number in the overall Fourier series. They contribute to the tail portion of the relatively sharp SD scattering. The overall average of column spacings influences the imaginary components of the Fourier coefficients of the SD scattering. This positions the static diffuse peak near the Bragg location. If this is compared with the quasiline peaks whose Fourier coefficients are determined from the severely distorted zone, a different average is found for this zone, which can give a shift further away from the Bragg position.

The form of $\varphi(n)$ still requires relative displacements between pairs of cells m_3, m_3' to be compiled at various separations of n. At this point, $\varphi(n)$ can be reduced to a direct calculation of displacements from a single defect. A re-examination of $\varphi(n)$, given by (33*b*), indicates that it is an autoconvolution expressed as a summation. As written, the diffuse intensity requires a series transform of $\varphi(n)$. Using this approach and knowing that the Fourier transform of an autoconvolution is the square of the Fourier transform of the convolution function, one obtains the desired form. The pair separation n is not required in the summation and we obtain

$$\varphi(h_3) = \sum_n \varphi(n)\exp(2\pi i n h_3) = c\left\{\sum_{m_1}\sum_{m_2}\sum_{m_3}[\exp(2\pi i l_0 Z_{m_3}) - 1]\exp(2\pi i m_3 h_3')\right\}^2. \quad (38)$$

If the terms of this series converge much more rapidly than N_n/N_3, the SD becomes

$$I_{SD}/N = F_{MP}^2 \exp(-2M)\sum_n \varphi(n)\exp(2\pi i n h_3), \quad (39)$$

since $N_n/N_3 \simeq 1$. Equation (38) contains a summation over projected displacements for all cells about a precipitate, considered singly rather than as pairs. Apart from the need to take a Fourier transform to obtain $\varphi(n)$, the numerical calculations are greatly simplified. For cells located at large distances from the precipitate but still at distances that allow m_3, m_3' pairs of cells to remain correlated, one finds $l_0 Z_{m_3} \ll 1$. These terms lead to a Huang scattering that is intermediate in sharpness, between a quasiline and its corresponding Bragg peak.

V. Integrated matrix intensities

The integrated intensities from the three components of scattering can be readily calculated from (37) by recognizing that the relative intensities are determined by letting $n=0$ in each of the Fourier coefficients. An examination of $\varphi(n)$ according to (33*b*) and (33*c*) for $n=0$ gives

$$\varphi(0) = 2c\sum_{m_1}\sum_{m_2}\sum_{m_3}[1-\cos(2\pi l Z_{m_3})] = 2M. \quad (40)$$

From (37), one readily finds the following partitioning of the matrix integrated intensities in terms of Bragg, static and quasiline contributions, as follows:

(i) Bragg $\exp(-2M)$, (41*a*)

(ii) static diffuse $2M\exp(-2M)$, (41*b*)

(iii) quasiline $1-\exp(-2M) - 2M\exp(-2M)$. (41*c*)

The partitioning of matrix intensities is illustrated in Fig. 1 in terms of Fourier coefficients at $L = nd = 0$, for calculations carried out for a Cu–Be alloy. An ellipsoid of revolution having semi-axes $C = 1.725$ Å, $A_1 = A_2 = 35$ Å and transformation strain of 12, 12 and -37.5% acting along each of the cubic axes is used as a representative precipitate. The $2M$ values are 0.9 and 1.3 for the (111) and (200) matrix peaks, respectively.

An examination of the Fourier coefficients and their dependence on column distance, L, shows that the coefficients for the (111) and (200) quasilines converge more rapidly than those representing SD scattering. Also, there is a very noticeable difference between the convergences along the (111) and (200) column directions. Anisotropy is observed in the displacement field from the ellipsoidal model, which gives a larger gradient of the interplanar spacing

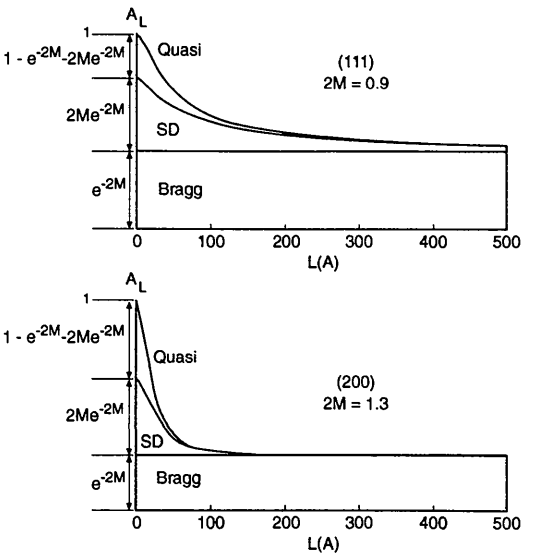

Fig. 1. Representative simulated Fourier coefficients from a severely distorted copper matrix containing disc-like beryllium-rich ellipsoids with semi-axes $A_1 = A_2 = 35$ and $C = 1.7$ Å. Transformation strains of 12, 12 and -37.3% are imposed at the precipitate zone along the cubic axes, which coincide with the ellipsoidal axes. (111) and (200) coefficients with $2M = 0.9$ and 1.3 are shown at various crystal distances, L, for quasiline, static diffuse and Bragg components.

along a [001] than along [111]. Separate representative shapes are shown in Fig. 2 for the sharp Bragg peaks, static diffuse scattering and quasilines for the (200) powder diffraction peak. For these simulations, the ellipsoid is strained by -20% along [001] and 0% along [100] and [010]. As one might expect from the convergence of the Fourier coefficients, the static diffuse peak is two to three times sharper than the corresponding quasiline. The quasiline shows the greatest shift away from the Bragg position while the static diffuse peak is located almost at the Bragg position.

The integrated intensity obtained with a diffractometer equipped with a monochromator from a polycrystalline material can be obtained from (41) by multiplying by the scaling function (see Schwartz & Cohen, 1987),

$$K_o K_i(2\theta),$$

with

$$K_i(2\theta) = (I_0 A_0 wh/\mu V_c^2) \times [(1+P\cos^2 2\theta)/(1+P)\sin^2\theta\cos\theta] j g_i \times \exp(-2M)_T \quad (42)$$

and K_0 = constant, I_0 = intensity of incident beam, A_0 = cross-sectional area of incident beam at the specimen. w and h are the receiver-slit width and height, respectively, μ is the overall linear absorption coefficient of the alloy, V_c is the volume of an average unit cell in the matrix, j is the multiplicity factor of the normal Bragg peak, g_i is the orientation correction factor for planes i if the sample has a texture ($g = 1$ if the sample is an ideal powder), P is the polarization factor, which is one if no monochromator is used,* 2θ is the diffraction angle for each of the three components for matrix scattering and $\exp(-2M)_T$ is the thermal factor for the matrix. The structure factor is given by (15*b*). If these equations are combined and integrated over σ^2/N, the integrated intensity for the matrix is partitioned according to

$$P_i/K_0 = K_i(2\theta_B)F_{MP}^2\exp(-2M) + K_i(2\theta_{SD})F_{MP}^2 2M\exp(-2M) + K_i(2\theta_Q)F_{MP}^2[1-\exp(-2M) - 2M\exp(-2M)]. \quad (43)$$

Typically, the peak separation between the three components is small enough to take a common $K_i(2\theta)F_{MP}^2$ for all three components when dealing with integrated intensities. However, this should be considered in terms of the details associated with each sample.

For experimental shape functions (measured with a 2θ axis), the intensity scaling in terms of the 2θ dependence is somewhat modified according to (see Schwartz & Cohen, 1987)

$$K_{os}K_{is}(2\theta) \quad (44a)$$

with

$$K_{is}(2\theta) = (I_0 A wh/\mu V_c^2 d) \times [(1+P\cos^2 2\theta)/(1+P)\sin^2\theta] j g_i \times \exp(-2M)_T. \quad (44b)$$

The constant K_{os} is not of interest because only relative intensities are of importance. All terms have been previoulsy defined, including d, which is given by (21).

The powder pattern describing the shape of the matrix intensity distributions is scaled by (44*a*). Combining this with (37) gives the Bragg, static diffuse and quasiline contributions:

$$[P_M(2\theta)/K_o\exp(-2M)] = K_{is}(2\theta_B)F_{MP}^2\sum_n (N_n/N_3)\exp(2\pi i n h_3) + K_{is}(2\theta_{SD})F_{MP}^2\sum_n (N_n/N_3)\varphi(n)\exp(2\pi i n h_3) + K_{is}(2\theta_Q)F_{MP}^2\sum_n (N_n/N_3)\{\exp[\varphi(n)]-1-\varphi(n)\} \times \exp(2\pi i n h_3). \quad (45)$$

Although the scaling terms K_{is} and the structure factors should strictly be calculated at the peak positions, the small separation normally allows these terms to be evaluated at the geometrical center of the overall intensity distribution from the matrix.

* If P is not known from experiment, it is conventionally taken to be $\cos^2 2\theta'$, where $2\theta'$ is the diffraction angle from the monochromator.

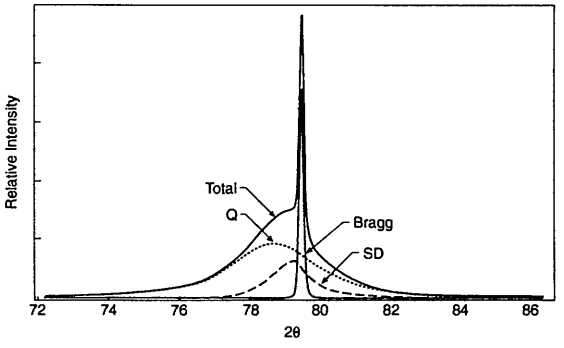

Fig. 2. Representative partitioning ($2M = 2.39$) of the simulated (200) matrix peak for Cr $K\alpha_1$ radiation into quasiline, static diffuse and Bragg components. An ellipsoid with semi-axes $A_1 = A_2 = 35$, $C = 7$ Å is used with transformation strains of 0, 0 and -20% acting along the plane of the ellipsoid and the perpendicular direction. These also coincide with the cubic axes for {100} precipitates.

VI. Precipitate scattering

In the general case where precipitate and void scattering overlap, they are not obviously separable. This

combination has been treated as a difference in their scattering amplitudes squared. It has the form of the classical Laue monotonic scattering but instead of dealing merely with the difference in scattering from two kinds of atoms, it involves a difference between the many atoms arranged into zones as precipitates and a similar but fictitious zone of matrix atoms. The latter look like an arrangement of matrix atoms over those distances required to form a void. Their positions and composition are defined in terms of the matrix atoms and its lattice. The local strain conditions are those existing in the matrix which develop as a result of precipitation. Because of the similarity with the matrix lattice over those distances associated with voids, void intensity overlaps matrix scattering. Furthermore, with the dominance of particle-size broadening, a separation into its diffuse components according to (34) is not useful because no single component is expected to be distinguishable or unique in its shape. Some, but not all, of the same discussion applies to the precipitate. For the early stages of precipitation, it is reasonable to assume that the displacement fields are continuous through each precipitate. However, each precipitate is subjected to an additive transformation strain that is not directly imposed upon a void. This additional transformation introduces a new lattice in both real and reciprocal space. Both the direct-void and precipitate intensities may be written most simply in the form

$$I_x/N = C_v(1-C_v)F_x^2[\exp(-2M)/N_v] \times \sum_{n_x}(N_n/N_3)\exp[\varphi(n)]\exp(2\pi i h_3^x), \quad (46)$$

with x referring to either voids or a precipitate. These appear in (16), along with a third term that requires both void and precipitate amplitudes. This cross term is nonzero in the general case with overlapping functions. It becomes more important as the differences between matrix and precipitate lattices become small and precipitate size is also small. If the precipitate scattering is sufficiently sharp or Bragg-like, scaling for the powder pattern shapes is obtained from (44*a*).

In order to treat precipitate scattering, fictitious void sites were introduced in order to be able to sum conveniently over all sites in the matrix. Subtracting these terms in the amplitude calculation leads to void scattering. In the present problem, the process of forming a void and refilling with a precipitate are interrelated and the combined scattering may be related to precipitation. Consequently, this combination will be called precipitate scattering rather than Laue scattering. Even when the overlap term can be neglected, one expects void as well as direct precipitate scattering even though void scattering is not readily measured. On this point, the estimated ratio of direct void intensity to matrix scattering at its peak is

$$C_v^2/(1-C_v)n_v.$$

For $C_v = 0.1$ and $n_v > 10$, the ratio at peak heights would be expected to be less than 0.001. Measurable void scattering would be expected beyond the range of the matrix scattering, which is more highly localized. The location of the direct precipitate scattering will, of course, depend on the transformation strain imposed upon the zone of precipitation, so that no general statements can be made.

Although the separation into three components is somewhat artificial, owing to the dominance of particle-size terms, (37) is of value in understanding asymmetry introduced by the imaginary component of $\varphi(n)$. An examination of the weighting factors given in (41) provides insight into trends brought about by increases in $2M$. As $2M$ increases, the contribution from the severely distorted zone increases. This influences $\varphi(n)$ and, therefore, the shape of the precipitate scattering. For intermediate $2M$, all three components influence the shape of the precipitate scattering; however, no single component introduces a strongly distinguishable feature. The weighted interplay of all three may introduce an asymmetry and peak shift.

As an additional complication, when the particle size becomes very small (< 30 Å), one must carry out an integration over a spherical surface in reciprocal space in order accurately to relate powder diffraction data with theory. Although such numerical calculations are readily carried out on a computer, it represents an added complication in the data-fitting procedure.

VII. Summary

A model has been discussed that deals with the X-ray scattering from randomly positioned precipitates in a finite and continuous crystalline matrix of fixed size. No conditions are placed upon the severity of the displacements. However, the fraction of precipitate centers must be small relative to the total number of lattice sites. The end result contains terms that describe the general scattering from the matrix, with zones of severe distortion, as well as the scattering from precipitates. This random-model calculation leads to the following conclusions:

(i) The intensity of matrix scattering is partitioned into three components; Bragg, static-diffuse (SD) and quasiline. As the severity of the displacements increase, the Bragg peaks are reduced, while the SD component can at first increase to a maximum before vanishing like the Bragg peaks. A quasiline is much broader and increases in intensity with the volume fraction of the severely distorted zone.

(ii) When they are observable, the Bragg peaks retain their sharpness, which is determined by the

overall size of the matrix lattice. This is independent of the size or number of precipitates, as well as of the severity of the field that surrounds them.

(iii) Scattering coherency from precipitates can influence the intensity from the matrix when the structures of the precipitate and matrix are similar enough to introduce overlapping amplitudes of scattering.

(iv) In the mixed–partitioned state only two matrix peaks may be apparent. One appears sharp and the second is broad. The sharp peak is a mixture of the Bragg and SD peaks, which tend to be located very near each other, while the broad peak is a quasiline. Consequently, matrix scattering may appear as a doublet.

(v) Precipitate scattering includes direct scattering from precipitates and voids as well as a cross term. The cross term may become negligible when no overlap occurs between the precipitate and void amplitude functions. In most cases, the shape of the precipitate scattering is primarily influenced by the size and shape of the precipitates. Displacement fields from other precipitates can interact and produce additional broadening. Partitioning in the case of precipitate scattering is not likely to be evident, although a peak shift and asymmetry resulting from strain may exist.

The author acknowledges his many discussions with Dr Satish Rao, dealing with the works of Krivoglaz and co-workers and the 1971 paper by Dederichs. These interactions on the diffraction effects of severely distorted lattices, as well as notes on these papers and computer simulations, were of considerable value in the author's development of the approach given in this paper. This work was made possible with the support of NSF Grant DMR-881 8013.

References

BARABASH, R. I. & KRIVOGLAZ, M. A. (1978). *Fiz. Met. Metalloved.* **45**, 7–18.

BARABASH, R. I. & KRIVOGLAZ, M. A. (1981). *Fiz. Met. Metalloved.* **51**, 903–916.

CULLITY, B. D. (1978). *Elements of X-ray Diffraction.* Reading, MA: Addison-Wesley.

DEDERICHS, P. H. (1970). *Phys. Rev. B*, **1**, 1306–1317.

DEDERICHS, P. H. (1971). *Phys. Rev. B*, **4**, 1041–1050.

DOBROMYSLOV, A. V. (1976). *Phys. Met. Metallogr.* **42**, 91.

DOBROMYSLOV, A. V. (1980). *Phys. Met. Metallogr.* **50**, 118.

GANZHUILA, N. N., KOZLOVA, L. YE. & KOKORIN, V. V. (1981). *Phys. Met. Metallogr.* **52**, 106–111.

HOLÝ, V. (1984). *Acta Cryst.* A**40**, 675–679.

IIDA, S., LARSON, B. C. & TISCHLER, J. Z. (1988). *J. Mater. Res.* **3**, 267–273.

KRIVOGLAZ, M. A. (1959). *Fiz. Met. Metalloved.* **7**, 650.

KRIVOGLAZ, M. A. (1960). *Fiz. Met. Metalloved.* **9**, 641.

KRIVOGLAZ, M. A. (1961). *Fiz. Met. Metalloved.* **10**, 169, 465.

KRIVOGLAZ, M. A. & HAO, T'YU (1969). *Fiz. Met. Metalloved.* **27**, 3–15.

LARSON, B. C., IIDA, S., TISCHLER, J. Z., LEWIS, J. D., ICE, G. E. & HABENSCHUSS, A. (1987). *Mater. Res. Soc. Symp. Proc.* **82**, 73–78.

LARSON, B. C. & SCHMATZ, W. (1974). *Phys. Rev. B*, **10**, 2307–2314.

MOSS, S., SPARKS, C. & ICE, G. (1992*a*). *Phys. Rev. B*, **45**, 2662–2676.

MOSS, S., SPARKS, C. & ICE, G. (1992*b*). *Phys. Rev. Lett.* **68**, 863–866.

SCHWARTZ, L. H. & COHEN, J. B. (1987). *Diffraction from Materials.* New York: Springer-Verlag.

TRINKHAUS, H. (1971). *Z. Angew. Phys.* **31**, 229.

WARREN, B. E. (1969). *X-ray Diffraction.* Reading, MA: Addison-Wesley.

Acta Cryst. (1993). A**49**, 781–789

Modelling Electrostatic Potential from Experimentally Determined Charge Densities. I. Spherical-Atom Approximation

BY NOUR-EDDINE GHERMANI, NOUZHA BOUHMAIDA AND CLAUDE LECOMTE*

Laboratoire de Minéralogie-Cristallographie et Physique Infrarouge–URA CNRS 809, *Université de Nancy* I, *Faculté des Sciences, BP* 239, 54506 *Vandoeuvre-lés-Nancy CEDEX, France*

(*Received* 25 *November* 1992; *accepted* 14 *May* 1993)

Abstract

Observations of the experimental electrostatic potential obtained from $X-X$ spherical electron density can be used to derive point charges centred on the atoms. This is applied to a pseudopeptide, *N*-acetyl-α,β-dehydrophenylalanine methylamide. The experimentally determined charges are consistent whatever the sampling points and 'follow' the atomic site when the conformation of the molecule

* To whom correspondence should be addressed.